The sensing characteristics of plasmonic waveguide with a ring resonator

Tiesheng Wu, Yumin Liu,* Zhongyuan Yu, Yiwei Peng, Changgan Shu, and Han Ye

State Key Laboratory of Information Photonics and Optical Communications, Beijing University of Posts and Telecommunications, Beijing 100876, China

microliuyumin@hotmail.com

Abstract: A surface plasmon polaritons (SPPs) refractive index sensor which consists of two metal-insulator-metal (MIM) waveguides coupled to each other by a ring resonator is proposed. The transmission properties are numerically simulated by finite element method. The sensing characteristics of such structure are systematically analyzed by investigating the transmission spectrum. The results indicate that there exist three resonance peaks in the transmission spectrum, and all of which have a linear relationship with the refractive index of the material under sensing. Through the optimization of structural parameters, we achieve a theoretical value of the refractive index sensitivity as high as 3460nmRIU^{-1}. Furthermore, this structure can also be used as a temperature sensor with temperature sensitivity of 1.36nm/°C. This work paves the way toward sensitive nanometer scale refractive index sensor and temperature sensor for design and application.

OCIS codes: (240.6680) Surface plasmons; (140.4780) Optical resonators; (230.0230) Optical devices; (130.6010) Sensors.

References and links

1. V. V. Temnov, G. Armelles, U. Woggon, D. Guzatov, A. Cebollada, A. Garcia-Martin, J.-M. Garcia-Martin, T. Thomay, A. Leitenstorfer, and R. Bratschitsch, "Active magneto-plasmonics in hybrid metal-ferromagnet structures," Nat. Photonics **4**(2), 107–111 (2010).
2. D. Martín-Becerra, J. B. González-Díaz, V. V. Temnov, A. Cebollada, G. Armelles, T. Thomay, A. Leitenstorfer, R. Bratschitsch, A. García-Martín, and M. U. González, "Enhancement of the magnetic modulation of surface plasmon polaritons in Au/Co/Au films," Appl. Phys. Lett. **97**(18), 183114 (2010).
3. F. Fan, S. Chen, X. H. Wang, and S. J. Chang, "Tunable nonreciprocal terahertz transmission and enhancement based on metal/magneto-optic plasmonic lens," Opt. Express **21**(7), 8614–8621 (2013).
4. A. Dolatabady, N. Granpayeh, and V. F. Nezhad, "A nanoscale refractive index sensor in two dimensional plasmonic waveguide with nanodisk resonator," Opt. Commun. **300**, 265–268 (2013).
5. V. E. Bochenkov, M. Frederiksen, and D. S. Sutherland, "Enhanced refractive index sensitivity of elevated short-range ordered nanohole arrays in optically thin plasmonic Au films," Opt. Express **21**(12), 14763–14770 (2013).
6. J. Zhu, J. J. Li, and J. W. Zhao, "Improve the refractive index sensitivity of coaxial-cable type gold nanostructure: the effect of dielectric polarization from the separate layer," J. Nanopart. Res. **15**(6), 1721 (2013).
7. S. Raza, G. Toscano, A. P. Jauho, N. A. Mortensen, and M. Wubs, "Refractive-Index Sensing with Ultrathin Plasmonic Nanotubes," Plasmonics **8**(2), 193–199 (2013).
8. A. Sun and Z. S. Wu, "A Hybrid LPG/CFBG for Highly Sensitive Refractive Index Measurements," Sensors (Basel) **12**(12), 7318–7325 (2012).
9. Y. Shen, J. H. Zhou, T. R. Liu, Y. T. Tao, R. B. Jiang, M. X. Liu, G. Xiao, J. Zhu, Z. K. Zhou, X. Wang, C. Jin, and J. Wang, "Plasmonic gold mushroom arrays with refractive index sensing figures of merit approaching the theoretical limit," Nat. Commun. **4**, 2381 (2013).
10. B. Gallinet and O. J. F. Martin, "Refractive index sensing with subradiant modes: A framework to reduce losses in plasmonic nanostructures," ACS Nano **7**(8), 6978–6987 (2013).
11. M. X. Ren, C. P. Pan, Q. Q. Li, W. Cai, X. Z. Zhang, Q. Wu, S. Fan, and J. Xu, "Isotropic spiral plasmonic metamaterial for sensing large refractive index change," Opt. Lett. **38**(16), 3133–3136 (2013).
12. F. Hao, P. Nordlander, Y. Sonnefraud, P. van Dorpe, and S. A. Maier, "Tunability of Subradiant Dipolar and Fano-Type Plasmon Resonances in Metallic Ring/Disk Cavities: Implications for Nanoscale Optical Sensing," ACS Nano **3**(3), 643–652 (2009).

#201878 - $15.00 USD Received 27 Nov 2013; revised 14 Mar 2014; accepted 14 Mar 2014; published 26 Mar 2014

13. Y. H. Fu, J. B. Zhang, Y. F. Yu, and B. Luk'yanchuk, "Generating and Manipulating Higher Order Fano Resonances in Dual-Disk Ring Plasmonic Nanostructures," ACS Nano **6**(6), 5130–5137 (2012).
14. J. H. Zhou, X. P. Xu, W. B. Han, D. Mu, H. Song, Y. Meng, X. Leng, J. Yang, X. Di, and Q. Chang, "Fano resonance of nanoparticles embedded in Fabry-Perot cavities," Opt. Express **21**(10), 12159–12164 (2013).
15. T. Cao and L. Zhang, "Enhancement of Fano resonance in metal/dielectric/metal metamaterials at optical regime," Opt. Express **21**(16), 19228–19239 (2013).
16. X. B. Kang, H. D. Li, J. Ding, and Z. G. Wang, "Fano resonance and step-like transmission via guide-mode resonance structure," Opt. Lett. **38**(5), 715–717 (2013).
17. K. Lodewijks, J. Ryken, W. V. Roy, G. Borghs, L. Lagae, and P. V. Dorpe, "Tuning the Fano Resonance Between Localized and Propagating Surface Plasmon Resonances for Refractive Index Sensing Applications," Plasmonics **8**(3), 1379–1385 (2013).
18. T. S. Wu, L. Wang, and Z. Wang, "A photonic crystal fiber temperature sensor based on Signac interferometer structure," Chin. J. Lasers **39**(11), 1114002 (2012).
19. L. Qi, C. L. Zhao, J. Y. Yuan, M. P. Ye, J. Wang, Z. Zhang, and S. Jin, "Highly reflective long period fiber grating sensor and its application in refractive index sensing," Sens. Actuators B Chem. **193**, 185–189 (2014).
20. M. M. Luo, Y. G. Liu, Z. Wang, T. T. Han, Z. Wu, J. Guo, and W. Huang, "Twin-resonance-coupling and high sensitivity sensing characteristics of a selectively fluid-filled microstructured optical fiber," Opt. Express **21**(25), 30911–30917 (2013).
21. C. Nicolaou, W. T. Lau, R. Gad, H. Akhavan, R. Schilling, and O. Levi, "Enhanced detection limit by dark mode perturbation in 2D photonic crystal slab refractive index sensors," Opt. Express **21**(25), 31698–31712 (2013).
22. S. C. Warren-Smith and T. M. Monro, "Exposed core microstructured optical fiber Bragg gratings: refractive index sensing," Opt. Express **22**(2), 1480–1489 (2014).
23. D. K. C. Wu, B. T. Kuhlmey, and B. J. Eggleton, "Ultrasensitive photonic crystal fiber refractive index sensor," Opt. Lett. **34**(3), 322–324 (2009).
24. J. J. Chen, C. W. Sun, and Q. H. Gong, "Fano resonances in a single defect nanocavity coupled with a plasmonic waveguide," Opt. Lett. **39**(1), 52–55 (2014).
25. B. W. You, J. Y. Lu, T. A. Liu, and J. L. Peng, "Hybrid terahertz plasmonic waveguide for sensing applications," Opt. Express **21**(18), 21087–21096 (2013).
26. E. A. Velichko and A. I. Nosich, "Refractive-index sensitivities of hybrid surface-plasmon resonances for a core-shell circular silver nanotube sensor," Opt. Lett. **38**(23), 4978–4981 (2013).
27. J. H. Zhu, X. G. Huang, J. Tao, X. P. Jin, and X. Mei, "Nanometeric plasmonic refractive index senor," Opt. Commun. **285**(13-14), 3242–3245 (2012).
28. X. S. Lin and X. G. Huang, "Tooth-shaped plasmonic waveguide filters with nanometeric sizes," Opt. Lett. **33**(23), 2874–2876 (2008).
29. T. B. Wang, X. W. Wen, C. P. Yin, and H. Z. Wang, "The transmission characteristics of surface plasmon polaritons in ring resonator," Opt. Express **17**(26), 24096–24101 (2009).

1. Introduction

Continuous improvements in nanofabrication and nanocharacterization capabilities have changed projections about the role that metals could play in the development of new optical devices [1]. SPPs are evanescent waves that propagate along a metal-dielectric interface. They can be laterally confined below the diffraction limit using subwavelength metal structures, rendering them attractive for the development of miniaturized optical devices [2]. In the past decades, varieties of sensors based on the surface plasmon resonance (SPR) have been widely investigated and studied [3–14], especially the refractive index sensing and SPR biosensing. Both SPPs and localized surface plasmon resonances (LSPRs) exhibit very interesting properties for sensing application due to their high degree of tenability and their susceptibility to the dielectric properties of the surrounding environment and structures [15–17]. Sensitivity is a key parameter to characterize sensor performance, increasing sensitivity can improve detection limit. At present, the state-of-the-art design of plasmonic sensor is plasmonic gold mushroom arrays, and the refractive index sensitivity of the plasmonic sensor is 1050nmRIU^{-1} [9]. Compared with the fiber sensor [18–23], the plasmonic sensor has small size, and it is ease to integration, but its sensitivity is not as high as that of fiber sensor (30100nmRIU^{-1}) [23]. Therefore, how to improve the sensitivity is a key issue in designing plasmonic sensor.

In this paper, a structure of two MIM waveguides coupled to each other by a ring resonator is proposed for refractive sensing and temperature sensing. Comparing to other plasmonic sensors, the advantage of this structure is high sensitivity. The sensitivity of this structure is close to 3.3 times larger than any reported plasmonic sensor device to date [3–17,

#201878 - $15.00 USD Received 27 Nov 2013; revised 14 Mar 2014; accepted 14 Mar 2014; published 26 Mar 2014

24–27]. The finite element method (FEM) with scattering boundary conditions is employed to simulate and research its sensing characteristics. In the simulation, this paper used commercial software COMSOL Multiphysics. The relationships between the resonance peaks in the transmission spectrum and the refractive index of the material under sensing, and temperature are analyzed. Additionally, the structural parameters of the sensor impact on sensitivity are analyzed to optimize the performance.

2. Model structure and theoretical analysis

The dispersion relation of the fundamental TM mode in an MIM waveguide (shown in the inset of Fig. 1) is given by [27, 28]

$$\varepsilon_{in}k_{z2} + \varepsilon_m k_{z1}\coth(ik_{z1}\omega/2) = 0, \tag{1}$$

with k_{z1} and k_{z2} defined by momentum conservations

$$k_{z1}^2 = \varepsilon_{in}k_0^2 - \beta^2, \tag{2}$$

$$k_{z2}^2 = \varepsilon_m k_0^2 - \beta^2, \tag{3}$$

where $\varepsilon_{in} = n^2$ is dielectric constant of the insulator, β is the propagation constant and $k_0 = 2\pi/\lambda_0$ is the free-space wave vector. Silver is chosen for its low absorption. The frequency-dependent complex relative permittivity of silver is characterized by the Drude model.

$$\varepsilon_m(\omega) = \varepsilon_\infty - \frac{\omega_p^2}{\omega^2 + i\omega\gamma}, \tag{4}$$

where $\varepsilon_\infty = 3.7, \omega_p = 9.1ev, \gamma = 18mev.$ The real part of the propagation constant β can be used to evaluate the effective index as n_{eff} = real (β/k_0). The dependence of effective index of MIM waveguide for SPPs on refractive index *n* is calculated and shown in Fig. 1.

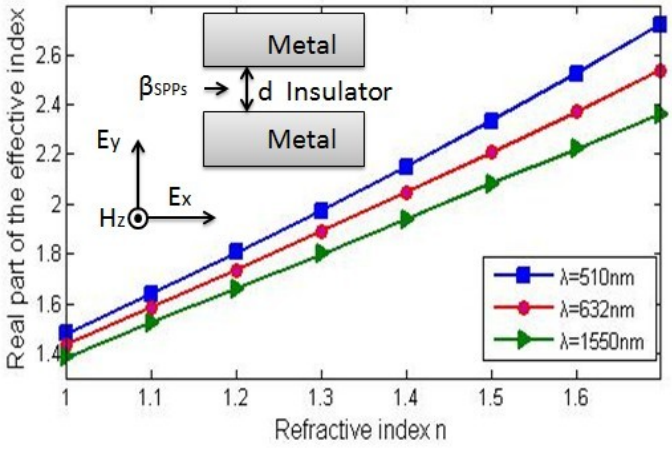

Fig. 1. Real part of the effective index versus the refractive index *n* of insulator in a slit MIM SPPs waveguide structure for different incident wavelengths.

The width of the slit *d* is set to be 50nm, the refractive index *n* of insulator varies from 1 to 1.7, and the metal is silver. From Fig. 1, it is easy to conclude that there is a linear

#201878 - $15.00 USD Received 27 Nov 2013; revised 14 Mar 2014; accepted 14 Mar 2014; published 26 Mar 2014

relationship between the effective refractive index and refractive index n of insulator for given wavelengths.

The nanometer scale SPPs waveguide sensor is schematically shown in Fig. 2(a). The device is composed of two MIM waveguides and a ring resonator. The material (liquid or gas) under sensing is filled in the slits and the ring resonator. The liquid filling can be achieved by capillary attraction. This structure can be made by template method, the light can be coupled into the sensor by nano-fiber and the output light can be detected by JY Confocal Raman Microscopy. In order to reduce the computational burden, 2D simulation is performed in this paper. The 2D structure is shown in Fig. 2(b), the widths of the slits and the ring are d, the outer (inner) radius of the ring is r_a (r_i) and we define the $r = (r_a + r_i)/2$ as radius of the ring. The coupling distance between SPPs waveguide and the ring resonator is w. The line S_1 and S_2 are perpendicular to the slits which are set to be 400nm, the distance between S_1 and S_2 is set to be 1200nm. For general cases, d, r and w are set to be 50nm, 170nm, and 10nm, respectively. The resonating wavelength of the ring resonator can be obtained theoretically by the equation [29]:

$$\frac{J_n^{'}(kr_a)}{J_n^{'}(kr_i)} - \frac{N_n^{'}(kr_a)}{N_n^{'}(kr_i)} = 0, \tag{5}$$

where $k = \omega(\varepsilon_0 \varepsilon_r \mu_0)^{\frac{1}{2}}$, μ_0 is the air permeability. $\varepsilon_r = n_{eff}^2 / \mu_0$ is the frequency-dependent effective relative permittivity. J_n and N_n are Bessel function of the first kind and second kind with order n respectively. $J_n^{'}$ and $N_n^{'}$ are derivatives of the Bessel functions to the argument (kr). In the following FEM simulations, scatter boundary conditions are used, the fundamental TM mode of the SPPs is excited by a port on the left slit. The transmission is defined to be $T = P_{out}/P_{in}$, where $P_{in} = \int PoavxdS_1$, $P_{out} = \int PoavxdS_2$, $Poavx$ is the x component of time-average power flow. The transmission spectra of the plasmonic sensor are obtained by parametrically sweeping the input wavelength of λ with step of 1nm.

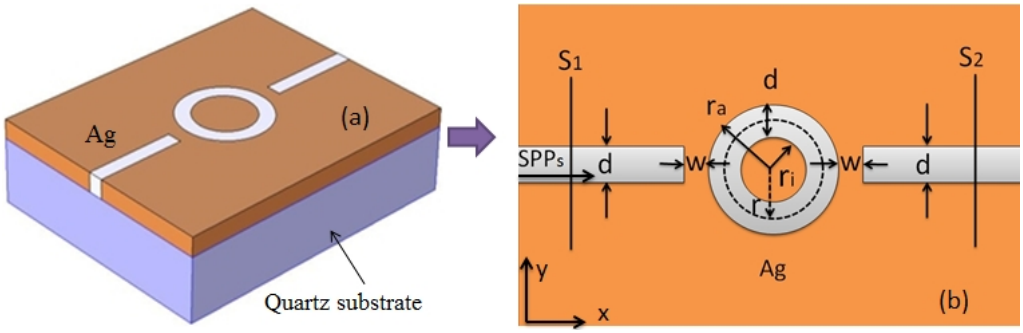

Fig. 2. Structure schematic of two slits MIM SPPs waveguide with a ring resonator. (a) Three-dimensional structure. (b) Two-dimensional structure.

3. Results and discussions

Figures 3(a)-3(d) show the transmission spectrum and the field distributions of the SPPs in the structure which filled with nothing, this means that the insulator is air with refractive index n = 1. The widths of the slits d are set to be 50nm, the coupling distance between the SPPs waveguides and the ring w is set to be 10nm, and the radius of the ring r is set to be 170nm. In Fig. 3(a), it is shown that there are three transmission peaks occur at the wavelengths of 526nm, 760nm and 1488nm, corresponding to the first, the second and the third resonance modes of the ring resonator. The transmission at peakIis over 85%, the

#201878 - $15.00 USD Received 27 Nov 2013; revised 14 Mar 2014; accepted 14 Mar 2014; published 26 Mar 2014

transmission at peakIIis about 78%, and the transmission at peakIII is about 55%, the loss of peak III is bigger than those of the other two. When satisfied ring resonance condition, the transmission reaches maximum. Figures 3(b), 3(c) and 3(d) show the contour profiles of the fields $|H_z|$ at different wavelengths. The field $|H_z|$ distributions in Figs. 3(c) and 3(d) correspond to the resonant peak wavelengths at the peak III and the peak II, respectively. In Fig. 3(b), the wavelength λ is 2000nm. The field $|H_z|$ distribution in the ring is very weak, and there is almost no magnetic field in the right-side slit, indicating that the wavelength cannot transport in this structure [29].

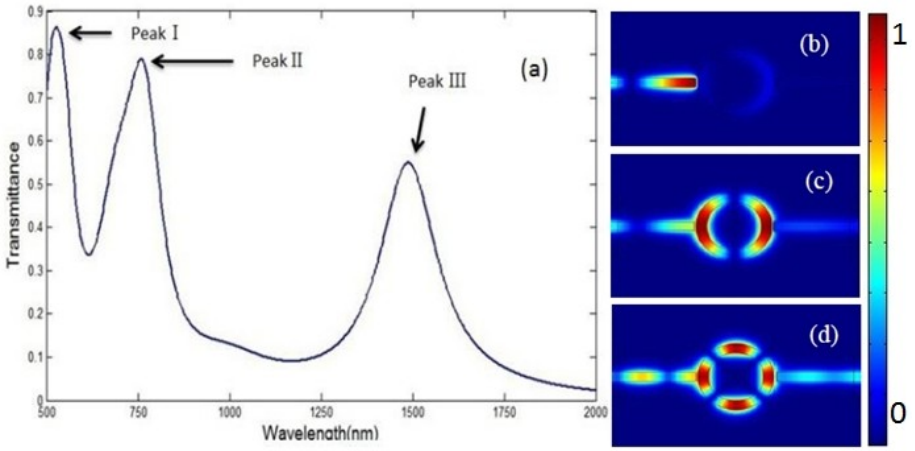

Fig. 3. (a) The transmission spectrum of the sensor structure. The contour profiles of field Hz of the device at different wavelengths of (b) λ = 2000nm, (c) λ = 1488nm, (d) λ = 760nm.

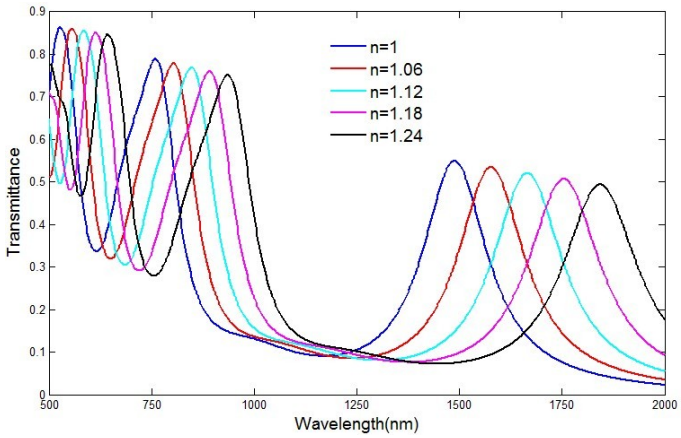

Fig. 4. The transmission spectrum of the structure for different refractive indices with d = 50nm, w = 10nm, and r = 170nm.

Next, we move on to study the influence of refractive index ***n*** on the peaks of the transmission spectrum. The refractive index ***n*** refers to the refractive index of the under-sensing insulator filled in slits and ring. Figure 4 shows the transmission spectrum of the sensor for different refractive indices from 1 to 1.24 with step of 0.06. As the refractive index increases, the transmission spectrum exhibits a red shift. The shift of peak III is the biggest, and the losses of all peaks are increased. Additionally, Fig. 5 depicts the three peaks of the transmission spectrum as a function of the refractive index of the material under sensing. The three peaks have a linear relationship with the refractive index n. With the refractive index

#201878 - $15.00 USD Received 27 Nov 2013; revised 14 Mar 2014; accepted 14 Mar 2014; published 26 Mar 2014

increasing, all of the peaks shift to longer wavelengths. The refractive index n is varied from 1 to 1.24, the shift of the peakIequals to 116.1nm, the shift of the peakIIequals to 175.9nm, and the shift of the peak III equals to 354.3nm. The sensitivity of refractive index sensor is defined as $d\lambda/dn$, resulting in 483.75nmRIU^{-1}, 732.92nmRIU^{-1} and 1476.25nmRIU^{-1} for the peakI, the peakII and the peakIII, respectively. According to the linear relationship between the peaks of the transmission spectrum and the refractive index as shown in Fig. 5, the refractive index of the material under sensing can be obtained from being detected the peak wavelength of the transmission spectrum, which is the sensing principle of the proposed device.

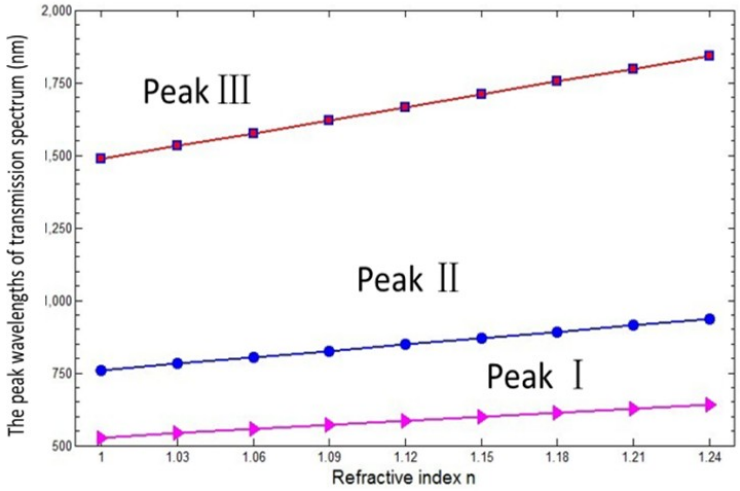

Fig. 5. The three peaks of transmission spectrum versus the refractive index n of the material under sensing.

To our knowledge, the refractive index sensitivity of the proposed device is high compared with previously reported SPPs waveguide sensors and LSPRs sensors [3–17, 24–27]. This structure is also appropriate to be used as a nanoscale temperature sensor. As a temperature sensor, we first need to find a liquid with high refractive index temperature coefficient, then fill it into two slits and ring, finally seal the liquid. Ethanol is adopted in the simulation. The temperature coefficient of ethanol is 3.94×10^{-4}. The refractive index of ethanol can be defined as

$$n = 1.36048 - 3.94\times10^{-4}(T - T_0), \tag{6}$$

where T_0 is the room temperature with a value of 20°C, T is the ambient temperature. The Eq. (6) displays the linear relationship between the refractive index of ethanol and temperature, while the shift of three transmission spectrum peaks have a linear relationship with the refractive index according to the above analysis. Therefore, the linear relationship between shift of three peaks and temperature retains. However, the three peaks of transmission spectrum shift to the shorter wavelengths when the temperature rising. Figure 6 shows the relationship between the shift of the peaks and the temperature. When the temperature rises from −100°C to 78°C, the peakI, the peakII and the peakIII shift 35.83nm, 54.28nm, 109.35nm, respectively. The sensitivity of temperature sensor is defined as $d\lambda/dT$, resulting in 0.19nm/°C, 0.29nm/°C and 0.58nm/°C for the peakI, the peakII and the peakIII, respectively. Compared to the traditional fiber optic sensors, the device can be eliminating the impact of stress and strain on the sensing. Because the melting point of ethanol is −114.3°C,

#201878 - $15.00 USD Received 27 Nov 2013; revised 14 Mar 2014; accepted 14 Mar 2014; published 26 Mar 2014

and the boiling Point is 78°C, so the device which filled with ethanol is suitable for low temperature sensing.

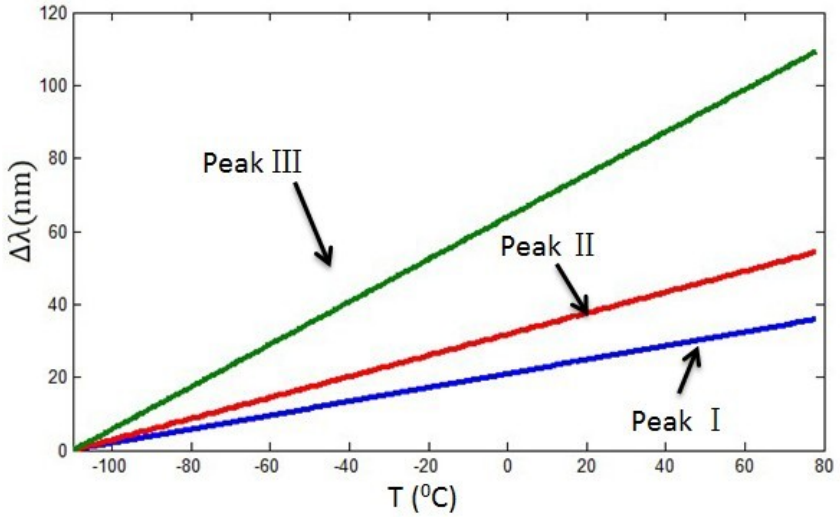

Fig. 6. The drift of the transmission peaks versus the temperature.

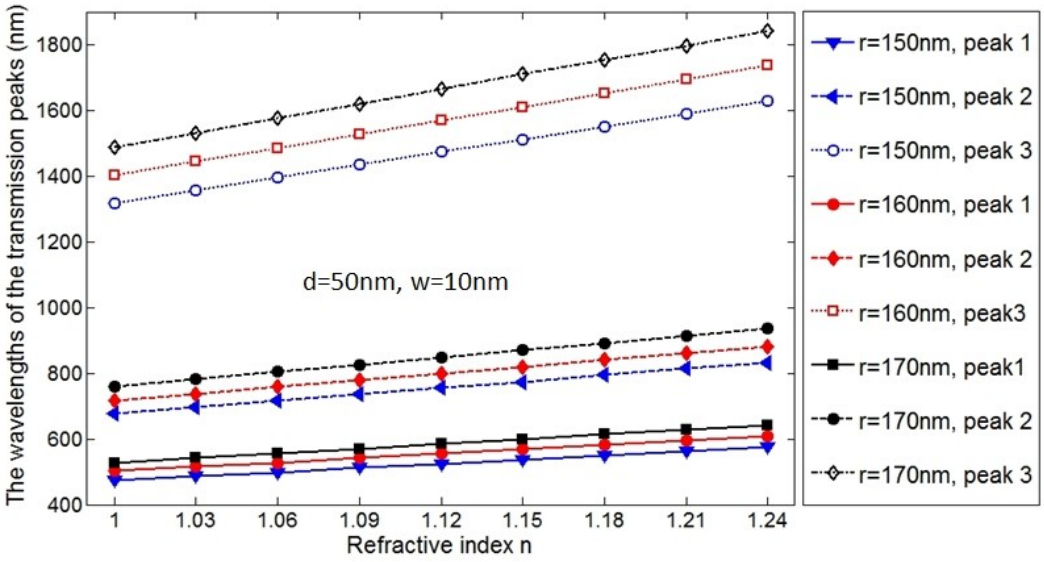

Fig. 7. The peaks of the transmission spectra versus the refractive index *n* with *r* = 150nm, *r* = 160nm, and *r* = 170nm.

Finally, the structural parameters of the device impact on sensing sensitivity are analyzed in order to improve the performance. Figure 7 demonstrates the peaks of the transmission spectra as a function of the refractive index for different radius of the ring with *r* = 150nm, *r* = 160nm, and *r* = 170nm, respectively. The radius of the ring can change the position of the peaks markedly, the wavelengths of the peaks become larger with the radius of the ring increasing, and it affects the refractive index sensitivity. While the radius of the ring is set to be 150nm, 160nm and 170nm, the refractive index sensitivity for the peakIis 416.67nmRIU^{-1}, 450.00nmRIU^{-1}, 483nmRIU^{-1}, correspondingly; the refractive index sensitivity for the peakIIis 645.83nmRIU^{-1}, 691.67nmRIU^{-1}, 732.92nmRIU^{-1}, correspondingly; the refractive

#201878 - $15.00 USD Received 27 Nov 2013; revised 14 Mar 2014; accepted 14 Mar 2014; published 26 Mar 2014

index sensitivity for the peakIII is 1300nmRIU^{-1}, 1391.67nmRIU^{-1}, 1476.25nmRIU^{-1}, correspondingly. The calculation results indicate that the refractive index sensitivity is improved with radius of the ring increasing. However, the disadvantage introduced by increasing the radius of the ring is the additional transmission loss. Figure 8 displays the peaks of the transmission spectra as a function of the refractive index for different widths of the waveguides and the ring with d = 30nm, d = 50nm and d = 70nm, respectively. The widths of the slits and the ring can also change the position of the peaks markedly, but it does not change the linear relationship between the transmission peaks and the refractive index n. While d is set to be 30nm, 50nm and 70nm, the refractive index sensitivity for the peakIis 558.33nmRIU^{-1}, 483.75nmRIU^{-1}, 441.68nmRIU^{-1}, correspondingly; the refractive index sensitivity for the peakIIis 845.83nmRIU^{-1}, 732.92nmRIU^{-1}, 683.33nmRIU^{-1}, correspondingly; and the refractive index sensitivity for the peakIII is 1816.68nmRIU^{-1}, 1476.25nmRIU^{-1}, 1366.68nmRIU^{-1}, correspondingly. The calculation results indicate that the refractive index sensitivity is lower with the widths of the slits and the ring increasing. As for the width of the coupling SPPs waveguide and the ring resonator w, simulation results show that it affects the positions of the peaks and loss, but it does not affect the sensing sensitivity. Therefore, we can improve the sensitivity of the SPPs waveguide sensor by means of increased the radius of the ring or decreased the widths of the slits and the ring.

Figure 9 shows the transmission spectrum of the structure for different radius and different refractive index. The transmission peaks indicate the peak III. w is set to be 10nm, and d is set to be 50nm. When r is set to 400nm, and refractive index increases from 1 to 1.1, the shift of the peak III is about 346nm. In the case, the refractive index sensitivity is as high as 3460nmRIU^{-1}, and the temperature sensitivity which filled with ethanol is as high as 1.36nm/°C. To our best knowledge, the theoretical value of the refractive index sensitivity is highest sensitivity reported in nanometre-sized sensors. It is close to 3.3 times larger than any reported plasmonic sensor device to date [3–17, 24–27].

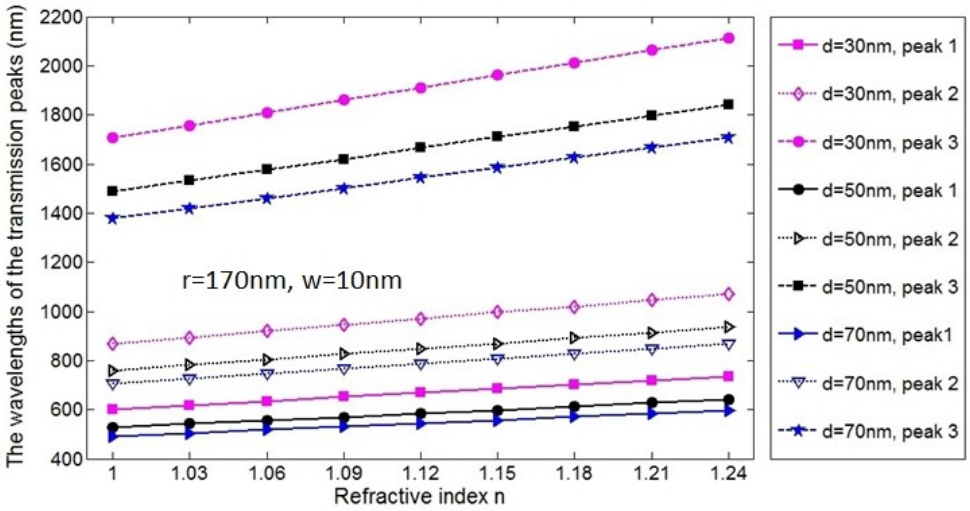

Fig. 8. The peaks of the transmission spectra versus the refractive index with d = 30nm, d = 50nm, and d = 70nm.

#201878 - $15.00 USD Received 27 Nov 2013; revised 14 Mar 2014; accepted 14 Mar 2014; published 26 Mar 2014

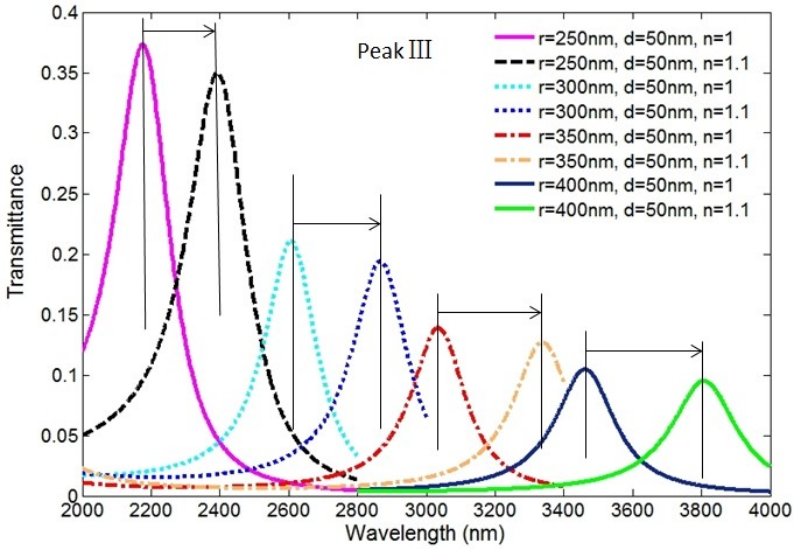

Fig. 9. Transmission spectra of the structure for different radius and different refractive index *n*

4. Conclusion

In summary, we have proposed a SPPs waveguide structure coupled by a ring resonator for refractive index sensing and temperature sensing. The sensing characteristics of the device are analyzed by 2D finite element method. The positions of transmission peaks have a linear relationship with both refraction index of the material under sensing and ambient temperature. The device not only has small size, which makes it easy to integration, but also it has a high sensing sensitivity. In addition, the device can be used as a tunable band-pass filter for a large wavelength range. The results have guiding significance for designing nanoscale high-sensitivity sensors.

Acknowledgments

The work was supported by the National Natural Science Foundation of China (61275201), the Program for New Century Excellent Talents in University of Ministry of Education of China (Grant No. NCET-10-0261), the Fund of State Key Laboratory of Information Photonics and Optical Communications (Beijing University of Posts and Telecommunications), P. R. China, and the Fundamental Research Funds for the Central Universities of Ministry of Education of China (Grant No. 2011RC0402), the Research Fund for the Doctoral Program of Higher Education of China (Grant No. 20100005110013), and the Opened Fund of the State Key Laboratory on Integrated Optoelectronics, Institute of Semiconductors, Chinese Academy of Sciences.

#201878 - $15.00 USD Received 27 Nov 2013; revised 14 Mar 2014; accepted 14 Mar 2014; published 26 Mar 2014